

Aborted jets and the X-ray emission of radio-quiet AGNs

G. Ghisellini¹, F. Haardt², and G. Matt³

¹ Osservatorio Astronomico di Brera, via Bianchi 46, 23807 Merate, Italy

² Dipartimento di Scienze di Como, Università dell’Insubria, via Valleggio 11, Como, 22100 Italy

³ Dipartimento di Fisica, Università degli Studi Roma Tre, via della Vasca Navale 84, 00146 Roma, Italy

Received 13 January 2003 / Accepted 30 September 2003

Abstract. We propose that radio-quiet quasars and Seyfert galaxies have central black holes powering outflows and jets which propagate only for a short distance, because the velocity of the ejected material is smaller than the escape velocity. We call them “aborted” jets. If the central engine works intermittently, blobs of material may be produced, which can reach a maximum radial distance and then fall back, colliding with the blobs produced later and still moving outwards. These collisions dissipate the bulk kinetic energy of the blobs by heating the plasma, and can be responsible (entirely or at least in part) for the generation of the high energy emission in radio-quiet objects. This is alternative to the more conventional scenario in which the X-ray spectrum of radio-quiet sources originates in a hot (and possibly patchy) corona above the accretion disk. In the latter case the ultimate source of energy of the emission of both the disk and the corona is accretion. Here we instead propose that the high energy emission is powered also by the extraction of the rotational energy of the black hole (and possibly of the disk). By means of Monte Carlo simulations we calculate the time dependent spectra and light curves, and discuss their relevance to the X-ray spectra in radio-quiet AGNs and galactic black hole sources. In particular, we show that time variability and spectra are similar to those observed in Narrow Line Seyfert 1 galaxies.

Key words. accretion, accretion disks – radiation mechanisms: thermal – X-rays: galaxies – galaxies: jets – galaxies: Seyfert

1. Introduction

One of the most popular scenario to explain the dichotomy between radio-loud and radio-quiet Active Galactic Nuclei (AGNs) assumes that only rapidly spinning black holes can give rise to the relativistic jets responsible for the radio emission and higher frequency non-thermal radiation observed in radio-loud objects (e.g. Blandford 1990). Therefore it was with some surprise that the first evidence for rapid rotation of a black hole came from a radio-quiet object, namely MGC-6–30–15. In the X-ray spectrum of this Seyfert 1 a broad iron line was observed by ASCA and *BeppoSAX* (Tanaka et al. 1995; Guainazzi et al. 1999) to be consistent with emission outside $6R_g$ ($R_g = GM/c^2$), i.e. the innermost stable orbit of an accretion disc around a static black hole. Recent XMM-Newton observations (Wilms et al. 2001; Fabian et al. 2002), however, indicate that the emission may extend well within $6R_g$, thus requiring a rotating black hole (the innermost stable orbit in the case of a maximally rotating black hole being R_g), and confirming the result obtained by Iwasawa et al. (1996) during a low flux state of the source observed with ASCA. Moreover, the very steep radial dependence of the iron line emissivity was interpreted by Wilms et al. (2001) as evidence for the extraction of the spin energy of a Kerr black hole, even if a pure

geometrical explanation (but still requiring a rotating black hole) is possible (Martocchia et al. 2002), provided that the illuminating source is very close to the black hole and resides on the symmetry axis. Similar evidence comes from XMM-Newton observations of the galactic black hole candidate XTE J1650–500 (Miller et al. 2002a).

Furthermore, Elvis et al. (2002) have recently suggested that the X-ray background requires a high efficiency of mass to energy conversion in the accretion process, possible if the black hole is rotating, but problematic in the case of a Schwarzschild black hole.

These results are at odds with the idea of a slowly spinning black hole in radio-quiet objects. On the other hand, and in a complementary way, radio-quiet objects are not radio-silent: even if the “dichotomy” between radio-loud and radio-quiet objects is currently under scrutiny (see e.g. White et al. 2000; Ivezić et al. 2002), all AGNs can produce radio emission at some level, which in turn is consistent with the idea that some sort of jet or outflow is always present, responsible to accelerate electrons to relativistic energy to radiate by the synchrotron process in the radio band. This idea has received recently fully support by VLBI imaging of Seyfert galaxies (Ulvestad 2003, and references therein) which revealed the presence of a mini-jet (at the sub-pc scale) in many Seyfert (radio-quiet) galaxies. In several cases it was also possible to detect the proper motions of knots in the jet, which appear to move with

Send offprint requests to: G. Ghisellini;
e-mail: gabriele@merate.mi.astro.it

subluminal apparent velocities of the order of a tenth of the speed of light.

Therefore it is conceivable to assume that all black hole plus accretion disk systems in AGNs can produce some kind of outflow or jet, but that only in a minority of cases (i.e. the “pure” radio-loud objects) the jet is successfully launched and accelerated to relativistic speeds. In the majority of cases, the jet is “aborted”, yet it is responsible for a relatively weak radio emission. The idea that all AGNs produce a jet is not new: among others, Falcke & Biermann (1995) suggested the jet-disk symbiosis for all AGNs, while Henri & Petrucci (1997) and Malzac et al. (1998) have argued that the initial part of a jet in a radio-quiet object can produce relativistic particles illuminating the disk. In these scenarios, however, the jet has either bulk relativistic motion or it contains very energetic particles, which are relativistic in the jet-comoving frame. In our scenario, as it will be explained below, the jet has sub-relativistic bulk velocities by assumption, and also most of the emitting electrons are thermal, with subrelativistic temperatures.

It is possible that a source which is usually radio-quiet may occasionally be successful in launching relativistic jets. This could explain the properties of galactic superluminal sources, in which major outflows sometimes occur. If this is true, these sources should be considered a crucial link between radio-loud and radio-quiet objects. In this respect, it is worth noting that in Galactic superluminal sources and Galactic black hole candidates there is often (even in radio-quiet states) the presence of a high energy X-ray power law, which may be associated with the emission from a jet, or at least from an outflow (as in the case of XTE 1118+480; Miller et al. 2002b).

The aim of this paper is twofold. First we will explore if the simplest “abortion mechanism” which comes into mind, i.e. a “jet” which does not succeed to reach the escape velocity, can work, at least qualitatively. Then we explore the possibility that the power initially in the jet and/or outflow can be used to heat the particles responsible to emit the X-ray flux from radio-quiet AGNs. In other words, we substitute the popular hot corona, possibly patchy, which sandwiches the accretion disk (i.e. Haardt & Maraschi 1991), with a single hot region on the rotation axis of the black hole, thought to be the site of the jet abortion. We then perform numerical simulations assuming to launch many blobs with slightly different velocities and time separations, calculate their trajectories and follow their evolution, accounting for the collisions occurring between them. This allows us to calculate the produced luminosity in each collision, and the total luminosity received by the observer in the likely case that more than one shell-shell collision is occurring at any given observing time. We will also study if the typical scattering optical depths and temperatures of the scattering particles in the aborted jet scenario are in agreement with what observed (Petrucci et al. 2001; Perola et al. 2002). Finally we will discuss our findings and derive some observational consequences enabling to test this scenario.

2. Escape velocity from a Kerr black hole

The mechanism to form, accelerate and collimate jets in radio-loud objects is not well understood, even if several proposals

exist in the literature (see e.g. the review by Lynden-Bell 2001). Here we do not attempt to propose a new mechanism. We simply postulate that in radio-quiet objects a similar mechanism is at work, but it is, on average, not able to impart to the outflowing material a bulk velocity larger than the escape velocity. We consider a blob of material in ballistic motion, and neglect the influence of magnetic fields and/or radiative fields (for calculations including the effect of accretion disk radiation see Vokrouhlický & Karas 1991).

The equation of motion of a test particle along the rotation axis of a Kerr hole is given by (see e.g. Vokrouhlický & Karas 1991):

$$\frac{d\beta}{dx} = - \frac{x^2 - a^2}{\beta\gamma^2(x^2 + a^2 - 2x)(x^2 + a^2)} \quad (1)$$

where $x \equiv R/R_g$, a is the (dimensionless) specific angular momentum (~ 1 for a maximally rotating Kerr hole), and $R_g = GM/c^2$ is the gravitational radius. Its solution is given by:

$$\gamma(x) = \gamma_0 \left[\frac{(x^2 + a^2)(x_0^2 - 2x_0 + a^2)}{(x_0^2 + a^2)(x^2 - 2x + a^2)} \right]^{1/2}. \quad (2)$$

It is then possible to find the escape velocity for a test particle having an initial velocity $c\beta_0$ at the distance $x_0 \equiv R_0/R_g$ on the rotational axis of a Kerr hole:

$$\beta_{\text{esc}} = \left[\frac{2x_0}{x_0^2 + a^2} \right]^{1/2} \quad (3)$$

yielding $\beta_{\text{esc}} = 1$ for $R = R_g$ and $a = 1$ (maximal Kerr hole), and for $R = 2R_g$ and $a = 0$ (Schwarzschild hole). Figure 1 shows the escape velocity β_{esc} as a function of the initial radius x_0 for different values of the angular momentum parameter a . Material with $\beta < \beta_{\text{esc}}$ will then outflow in the radial direction reaching a maximum distance from the black hole, and then it will fall back. The maximum distance above the hole where the motion inverts, x_{max} , can be found setting $\gamma(x_{\text{max}}) = 1$ in Eq. (2), to find

$$x_{\text{max}} = \frac{k + \sqrt{k^2(1 - a^2) + 2ak - a^2}}{k - 1}; \quad (4)$$

$$k \equiv \frac{x_0^2 + a^2}{\gamma_0^2(x_0^2 + a^2 - 2x_0)}.$$

Figure 2 shows for illustration some examples of “trajectories”.

3. Jet power and internal shocks

In this section we discuss the basic features of our model. In order to have an analytical treatment, we will consider here only a simple case, while the more realistic, but much more complex case, will be treated numerically in Sect. 5.

The total power carried by the jet is

$$L_j = \Gamma_0 \dot{M}_{\text{out}} c^2 \quad (5)$$

where Γ_0 is the bulk Lorentz factor corresponding to the initial velocity of the jet, and \dot{M}_{out} is the mass ejection rate, which is

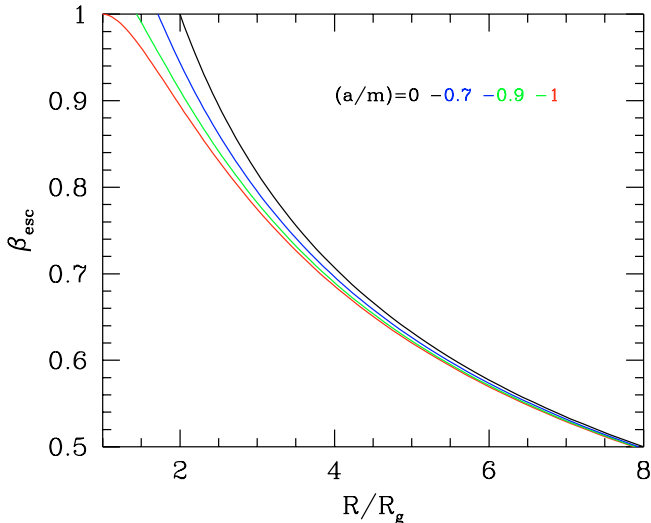


Fig. 1. Escape velocity as a function of distance from the black hole and for $a = 0, 0.7, 0.9$, and 1 , from top to bottom.

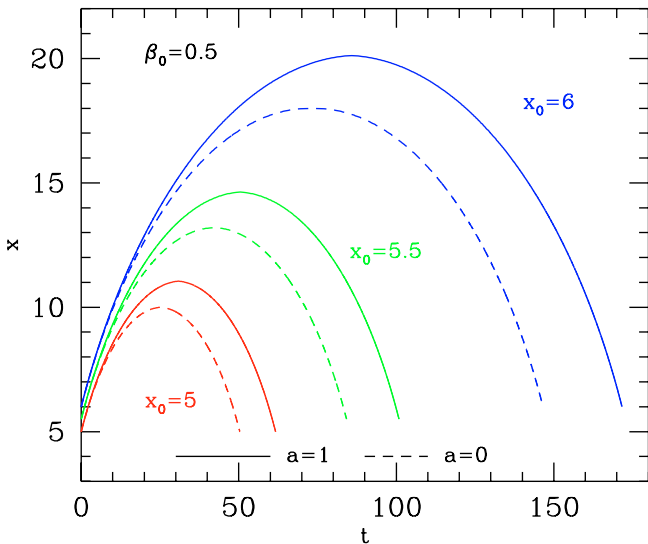


Fig. 2. Trajectories of test particles in motion along the rotation axis of an extreme Kerr hole ($a = 1$, solid lines), and Schwarzschild (dashed lines), for the initial radii $x_0 \equiv R/R_g = 5, 5.5$, and 6 , as labeled. The initial velocity is $\beta_0 = 0.5$. Time is measured in units of the initial light crossing time R_0/c .

in principle a free parameter of the model, but it can be constrained by the observed ratio between the X-ray and UV luminosity. A fraction η_j of L_j will be transformed into radiation.

We propose that the central engine producing the jet is not working continuously, but intermittently, leading to collisions between blobs of material launched at different times, and moving with slightly different velocities. In the case of successful jets this will lead to the formation of “internal shocks”, first proposed by Rees (1978) for the jet of the radio-galaxy M 87, later proposed to explain the prompt emission of gamma ray bursts (Rees & Mészáros 1992; Rees & Mészáros 1994; Sari & Piran 1997), and recently proposed again to explain the entire spectral energy distribution of all radio-loud AGNs (Ghisellini 1999; Spada et al. 2001). In this scenario the shells collide at a

typical distance R_{diss} from the black hole given by $R_{\text{diss}} \sim \Gamma^2 R_0$, where Γ is the average bulk Lorentz factor of the shells and R_0 is the initial shell–shell separation. In the case of aborted jets the intermittency of the process will lead to collisions between a blob already falling backwards to the hole and a blob still moving upwards. There is no need, in this case, to assume slightly different velocities, since the collisions will occur anyway. The details of the collision depend upon the initial velocities and the typical “launching” site, which is related to the time needed to accelerate a blob.

There may be a range of locations R_{coll} where collisions preferentially take place, depending on the initial time separation of two consecutive shells, their initial velocity β_0 , and on the initial launching site R_0 . These parameters, together with the angular momentum of the Kerr hole, determine R_{coll} , which in turn determines the amount of bulk kinetic energy which can be dissipated. Larger R_{coll} in fact correspond to smaller kinetic energies (and larger potential ones). Figure 3 shows for illustration simple examples of the velocity and kinetic energy of two colliding shells, as a function of R_{coll} . In these examples we assume the same mass, initial velocity and launching site for all blobs.

In a more realistic case, R_{coll} will be dependent partly on the exact values of the initial parameters, and partly on the past history of the process, in the sense that a falling blob may interact with more than one later blobs (including some which may have $\beta > \beta_{\text{esc}}$). Interestingly, the power which can be extracted is a function of the dissipation distance, since the more powerful collisions will be between just launched blobs and falling blobs with a back velocity of the order of the initial one, and this will occur closest to the hole (see Fig. 3). We also stress that in these examples we have only treated the simplest possible case, neglecting in particular the interaction of the blob with the radiation produced by the accretion disk and the motion off the angular momentum axis.

With our simple approximations, the dissipated power is the entire kinetic power of the shells when they collide, since they have equal and oppositely directed velocities. Thus the total momentum is zero if the shells have, as we assume, equal masses. We can then link the radiative efficiency of the process to the kinetics of the collision through:

$$\eta_j = \epsilon_e \frac{\Gamma_{\text{coll}} - 1}{\Gamma_0 - 1} \quad (6)$$

where ϵ_e is the fraction of the collisional energy radiated by the electrons (and possibly electron–positron pairs), and Γ_{coll} is the bulk Lorentz factor when the blobs collide. We do not know what is the dominant acceleration mechanism transforming ordered into random energy, and this precludes to know with confidence what fraction of the total energy goes to the emitting electrons (and possibly positrons), and what fraction is instead given to protons and to magnetic field. Equipartition between protons, electrons and magnetic field would result in a value of $\epsilon_e \approx 1/3$. The value of η_j can be calculated for any assumed value of ϵ_e from Fig. 3 and Eq. (6).

Observationally, the X-ray luminosity is of the order of 10–50 per cent of the luminosity in the optical–UV (e.g. Walter & Fink 1993), thought to be produced by the accretion disk, for

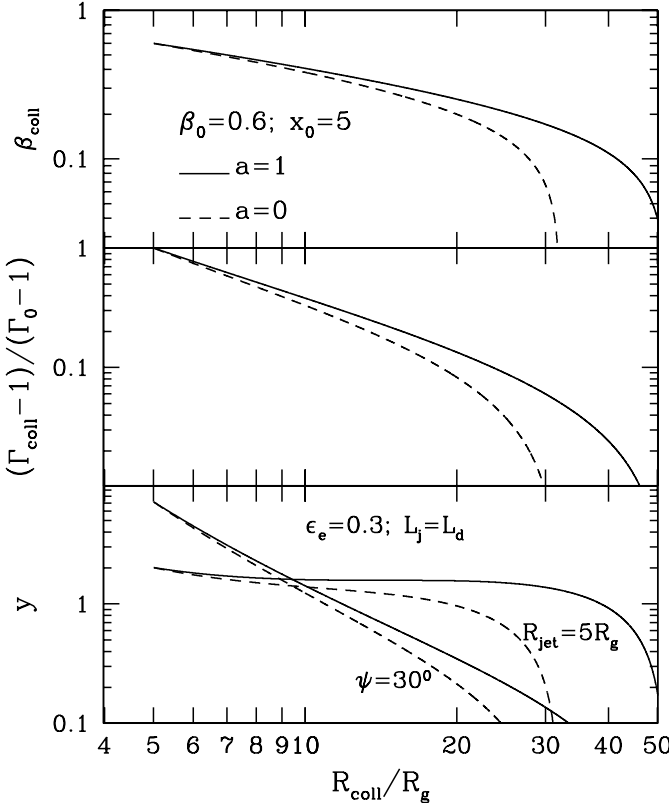


Fig. 3. Consecutive shells collide at different distances from the black hole and with different velocities. In the collision they dissipate their kinetic energy, proportional to $\Gamma_{\text{coll}} - 1$. An initial distance $x_0 = 5$ and initial velocity $\beta_0 = 0.6$ is assumed. Solid lines refer to a maximally rotating Kerr hole, dashed line to a Schwarzschild black hole. Top panel shows the velocity of the shells when they collide; the mid panel shows the total dissipated energy, which is greater closer of the hole; the bottom panel shows the Comptonization y parameter, calculated following Eq. (12), and assuming, as labeled, $L_j = L_d$ and $\epsilon_e = 0.3$. We show the case of shells of fixed dimensions (set to $5R_g$ in this example) or expanding as $r_j = \psi R_{\text{coll}}$, where we have used $\psi = 30^\circ$.

which $L_d = \eta_d \dot{M}_{\text{in}} c^2$. Here \dot{M}_{in} is the mass accretion rate and η_d is the accretion efficiency.

If all the X-ray luminosity L_X comes from the aborted jet, i.e. $L_X = \eta_j L_j$, while $L_d \sim L_{\text{UV}}$, we have:

$$\frac{\dot{M}_{\text{out}}}{\dot{M}_{\text{in}}} = \frac{1}{\Gamma_0} \frac{\eta_d}{\eta_j} \frac{L_X}{L_{\text{UV}}}. \quad (7)$$

Since Γ_0 is always of order unity, we have that $\dot{M}_{\text{out}} \sim (L_X/L_{\text{UV}}) \dot{M}_{\text{in}} \sim 0.1 \dot{M}_{\text{in}}$ if the jet and the accretion efficiencies are of the same order.

4. The X-ray emission

In this section we again discuss the very simplified case of the collision of two oppositely directed blobs having the same mass and same velocity (in modulus), in order to understand the basics of the interaction with an analytical treatment.

4.1. Formation of the X-ray continuum

Having established that the simple aborted jet scenario discussed above can in principle account for the energetics of the X-ray emission, we must now check whether the physical parameters of the aborted jets, i.e. its optical depth and temperature, are consistent with the X-ray spectral constraints.

The accelerated leptons are embedded in a very large radiation energy density produced by the close-by accretion disk and by the local magnetic field possibly enhanced by the collision. Under these conditions, the most efficient radiation processes are Inverse Compton scattering and cyclo-synchrotron emission. We will see below that energy balance ensures that the equilibrium lepton energy is mildly relativistic at most. This implies that the cyclo-synchrotron process occurs in the self-absorbed regime and then does not contribute to the cooling. This process could however be important for establishing an electron Maxwellian distribution in a timescale shorter than the dynamical time (Ghisellini et al. 1998). For simplicity, we then assume that the energized leptons have a thermal energy distribution. It is worth noting that a distribution which is not a perfect Maxwellian, but has a well defined mean energy, such as a distribution with a well defined peak energy, or a power law energy distribution ($\propto E^{-n}$) with $n > 3$, give rise to a Comptonization spectrum which cannot be distinguished by the one formed by a perfect Maxwellian (see e.g. Ghisellini et al. 1993).

To find the typical average energy $\gamma m_e c^2$ of the emitting leptons, we balance radiation losses with the energy gains due to the shell-shell collision process. The inverse Compton cooling rate is:

$$\dot{E}_c = \frac{4}{3} \sigma_{\text{T}} c U_r \gamma^2 \beta^2 \quad (8)$$

where U_r is the radiation energy density of the disk emission. The heating rate due to the shell-shell collision is

$$\dot{E}_h = \frac{\eta_j L_j}{N_e} \quad (9)$$

where N_e is the total number of leptons in the emitting region. Balancing heating and cooling we have:

$$\gamma^2 \beta^2 = \frac{3}{4} \frac{\eta_j L_j}{\sigma_{\text{T}} c N_e U_r}. \quad (10)$$

Assume that the “jet” emitting region has a transverse size r_j and a width Δr_j . Its scattering optical depth is

$$\tau_{\text{T}} = \frac{N_e}{f r_j^2 \Delta r_j} \sigma_{\text{T}} \Delta r_j \quad (11)$$

where f is a geometry dependent factor (e.g., $f = 4\pi/3$ for a sphere).

If $\tau_{\text{T}} \lesssim 1$, the Comptonization parameter is $y \equiv (4/3) \tau_{\text{T}} \gamma^2 \beta^2$. In this case we have:

$$y = \frac{\eta_j L_j}{f r_j^2 c U_r}. \quad (12)$$

The energy density U_r depends on the specific geometry of the system and on the accretion luminosity. Note that L_d should

always be greater than $\eta_j L_j/2$, since about half of the jet produced luminosity impinges on the accretion disk. However, observations typically give $L_d \sim L_{UV} \sim 10L_X$, suggesting that the accretion–produced luminosity is dominating with respect to the jet luminosity intercepted and reprocessed by the disk. For simplicity, let us assume a Newtonian disk producing a total power L_d , which has a minimum radius r_* . Per unit surface area the dissipated flux is (e.g., Frank et al. 1985):

$$D(r) = \frac{3L_d r_*}{4\pi r^3} \left[1 - \left(\frac{r_*}{r} \right)^{1/2} \right], \quad (13)$$

where r is the radial coordinate of the accretion disk. The intensity $I(r)$ corresponding to this dissipation is $I(r) = D(r)/\pi$. At the location R_{coll} the total radiation energy density produced by the disk is

$$\begin{aligned} U_r(R_{\text{coll}}) &= \frac{2\pi}{c} \int_0^{\mu_{\text{max}}} I(r) d\mu \\ &= \frac{3L_d r_* R_{\text{coll}}}{2\pi c} \int_{r_*}^{\infty} \frac{1 - (r_*/r)^{1/2}}{r^2 (R_{\text{coll}}^2 + r^2)^{3/2}} dr \end{aligned} \quad (14)$$

where $\mu \equiv \cos \theta$ and θ is the angle with respect to the normal of the accretion disk.

Inserting $U_r(R_{\text{coll}})$ in Eq. (12) we can calculate the Comptonization y parameter. In the bottom panel of Fig. 3 we show, as illustration, how y changes as a function of R_{coll} if the shell remains of the same dimension (i.e. $r_j = \text{constant}$) or if instead it expands as a cone of semiaperture angle ψ (in this case we have assumed $r_j = \psi R_{\text{coll}}$). In both cases we show the behavior for a maximally rotating Kerr hole ($a \sim 1$) and for a Schwarzschild hole ($a = 0$).

A constant r_j implies an almost constant y -parameter. This is because η_j and U_r decrease with R_{coll} in approximately the same way. If the shells expand, instead, y decreases because the optical depth of the scattering electrons decreases as $\tau_T \propto r_j^{-2} \propto R_{\text{coll}}^{-2}$.

Equation (12) also gives the y -parameter in the classical case of an homogeneous corona sandwiching the accretion disk. Assuming that the jet dissipates the entire available gravitational energy, and that half of it is reprocessed by the accretion disk, we can substitute $\eta_j L_j$ with L_X , L_d with $L_X/2$. Furthermore, the disk radiation energy density in this case can be approximated by $U_r = 2L_X/(\pi r_j^2 c)$. Setting $f = \pi/2$, we finally obtain $y = 1$.

4.2. Are electron–positron pairs important?

The assumption that the jet carries a power L_j in the form of kinetic energy links the amount of transported power with the scattering optical depth. On the other hand, τ_T may not be linearly proportional to L_j , because of the possible presence of electron positron pairs, which contribute fully to the scattering optical depth but not so much to the jet power (if protons are also present and are dominating the jet inertia). We will therefore estimate first a lower limit to the scattering optical depth assuming no pairs, and then we will make some considerations to evaluate the contribution of pairs.

To calculate the initial optical depth of each blob, without the contribution of pairs, we first consider the kinetic energy carried by each blob, and use it to find its mass M_i :

$$M_i = \frac{L_j \Delta t}{\Gamma_{i,0} c^2} \quad (15)$$

where Δt is the time interval between two consecutive blob ejection. All the values of the quantities in Eq. (15) have to be considered as average values. The total number of electrons contained in each blob is therefore $N_e = M_i/m_p$ if the jet is made by an electron–proton plasma. Inserting this value in Eq. (11) we get:

$$\tau_T = \frac{\sigma_T L_j \Delta t}{m_p c^2 f r_j^2 \Gamma_{i,0} c^2} = \frac{4\pi}{f \Gamma_{i,0}} \frac{L_j}{L_{\text{Edd}}} \left(\frac{r_g}{r_j} \right)^2 \frac{\Delta t}{r_g/c}. \quad (16)$$

For the second equality, we have used the jet luminosity in units of the Eddington one, the blob size in units of r_g and time in units of r_g/c . In this way it becomes clear that the optical depth (without the contribution of pairs) is scale invariant with respect to the mass of the black hole. Furthermore, it is also clear that, for r_j of the order of the gravitational radius, for jet kinetic powers of order of 0.01–0.1 of the Eddington luminosity and for time intervals of a few times r_g/c the initial optical depth is of order of 0.01–0.1.

If the jet, instead, is made by a pure electron–positron plasma, then the initial value of the optical depth is a factor m_p/m_e greater, and consequently τ_T becomes much larger than unity. In this case the pairs annihilate efficiently, since the annihilation timescale is of order of $r_j/(c\tau_T)$, and most of the kinetic power of the jet is lost through annihilation. We conclude that if the jet is energetically important, then its inertia must be given mainly by protons.

We stress that there is a remarkable feature in the model, which is the link between the kinetic power and the amount of electrons and protons carried by the jet. In pair–corona models, the optical depth of the corona has a lower limit given by the created pairs (Haardt & Maraschi 1991). Here, instead, the limit is given by the jet power.

We can also estimate the possible importance of pairs created during the emission phase. In other words, when primary electrons are heated by the shell–shell collision, they can emit photons above the pair production threshold: if the source is sufficiently compact, these photons create pairs which increase the optical depth and contribute to the emission.

The effects of pairs have been studied in detail assuming a steady source in pair equilibrium (creation equal annihilation, Svensson 1984). Our source is probably never in steady state, but we can use the results of these studies as a guide to estimate the relevant pair optical depths and temperatures. The optical depth due to pairs, produced in steady state and in pair equilibrium without pair escape, can be approximated by (Haardt 1994):

$$\tau_{\pm} \approx 0.016 (\ell_x)^{0.56}, \quad 20 \lesssim \ell_x \lesssim 200 \quad (17)$$

where $\ell_x \equiv \sigma_T L_X/(r_j m_e c^3)$ is the compactness of the X–ray radiation produced by a shell–shell collision, and can be considered equal to $\eta_j \ell_j$. This equation assumes that the radiation

process is Comptonization, and is valid assuming spectral indices α_x of the Comptonized spectrum around unity. The range of X-ray compactnesses relevant for Seyfert galaxies is within the same range of the compactness relevant for the accretion disk emission, i.e. $\ell_x \sim 1-10$.

By comparing Eq. (17) with Eq. (16) we see that pairs should be unimportant for compact jets. Furthermore, as will be clear in the following section, the optical depth of each shell is increasing each time it collides with another one (if lateral expansion can be neglected), driving the typical optical depth to values a factor ~ 10 larger than the initial value. We then conclude that electron positron pairs do not play a fundamental role in this scenario.

5. Numerical simulations

We have discussed so far the illustrative and very simple case of a pair of blobs of equal mass, equal launching site and initial velocity, colliding at different distances from the black hole. In a more realistic case, we should assume that the time interval Δt between the launch of consecutive blobs is variable, as well as the blob mass, initial velocity, and their launching site. To simulate this, we use a Monte Carlo code which extracts the initial quantities within an assigned distribution. We have then assumed a Gaussian distribution for the initial velocity (i.e. we assign a mean value and a width σ), while for the time interval Δt we assume a Poisson distribution. We have then considered the case of a Gaussian distribution of the blob masses, leading to initially different kinetic energies of the blobs, and the case of equal kinetic energies for all blobs. In this latter case the mass is therefore determined by the blob velocity.

We follow the trajectory of all blobs, and when they collide we calculate the corresponding dissipation through the equation of conservation of energy and momentum:

$$\Gamma_1 m_1 + \Gamma_2 m_2 = \Gamma_f (m_1 + m_2 + \epsilon' / c^2) \quad (18)$$

$$\Gamma_1 \beta_1 m_1 + \Gamma_2 \beta_2 m_2 = \Gamma_f \beta_f (m_1 + m_2 + \epsilon' / c^2). \quad (19)$$

In these equations the subscripts 1 and 2 stand for the two blobs, $\Gamma = (1 - \beta^2)^{-1/2}$ is the bulk Lorentz factor just before the collision and Γ_f if the final Lorentz factor of the two blobs just after the collision. ϵ' is the dissipated energy, calculated in the frame comoving with the merged blobs. Hereinafter primed quantities are calculated in this frame. A completely anelastic collision is assumed. The two unknowns are β_f (or Γ_f) and ϵ' which are given by:

$$\beta_f = \frac{\Gamma_1 \beta_1 m_1 + \Gamma_2 \beta_2 m_2}{\Gamma_1 m_1 + \Gamma_2 m_2} \quad (20)$$

$$\frac{\epsilon'}{c^2} = [m_1^2 + m_2^2 + 2m_1 m_2 \Gamma_1 \Gamma_2 (1 - \beta_1 \beta_2)]^{1/2} - m_1 - m_2. \quad (21)$$

A fraction ϵ_e of ϵ' is given to the radiating electrons, making the X-ray luminosity, as observed in the comoving frame:

$$L'_x \simeq \epsilon_e \frac{\epsilon'}{t'_{\text{diss}}} \quad (22)$$

where t'_{diss} is the time needed to radiate the energy $\epsilon_e \epsilon'$. In the dense seed photon environments we are considering, the electron radiative cooling time is fast, always shorter than blob-blob crossing time t'_{cross} . We then assume that $t'_{\text{diss}} \simeq t'_{\text{cross}}$. We compute t'_{cross} in the frame of one of the two blobs,

$$t'_{\text{diss}} \simeq t'_{\text{cross}} = \frac{\Delta r_j}{c} \frac{1 - \beta_1 \beta_2}{|\beta_1 - \beta_2|}. \quad (23)$$

We identify L'_x with the “radiative jet luminosity” $\eta_j L_j$ of Eq. (12) and derive the corresponding value of the Comptonization parameter y .

At any time, the observer can see more than one collision, and therefore we calculate, at any time, the number of colliding shells. We then sum up their luminosities and assume, for each collision, a triangular luminosity profile with symmetric rise and decay timescales (each of duration t_{diss}), whose time integral is equal to the energy dissipated by the electrons. The observed luminosity produced by each collision is modified by special relativistic effects, which we account for introducing the Doppler beaming parameter:

$$\delta \equiv \frac{1}{\Gamma_f (1 - \beta_f \cos \theta)} \quad (24)$$

where θ is the viewing angle and β_f must be considered with its sign (positive for shells approaching the observer). We then multiply the comoving luminosity by δ^4 and divide the intrinsic timescale by δ . Note that δ can be greater or smaller than unity, depending on β_f and θ . We take into account time dilation due to general relativity, by dividing intrinsic times by the factor $(1 - 2R_g/R)^{1/2}$, where R is the distance from the black hole, and multiplying intrinsic frequency by the same factor. We call the resulting observed luminosity L_x^{obs} .

The luminosity is assumed to be produced when two shells merge. For simplicity, we assume that the entire produced radiation is emitted once the velocity of the merged shell has already reached the final value, and use this velocity to calculate the appropriate special relativistic effects. We then continue to follow the merged shells until a new collision occurs, or until it reaches a distance from the black hole equal or less than the initial one.

Note that the mass of a generic blob increases for each collision, and in the absence of side expansion this implies a corresponding increase of the scattering optical depth.

We have also taken into account the additional electron heating due to Coulomb collisions between protons and electrons, occurring on the timescale t'_{ep} given by (e.g. Stepney 1983)

$$t'_{\text{ep}} \sim \frac{\Delta r_j}{c \tau_T} \frac{m_p / m_e}{\ln \Lambda} \left(\frac{kT_e}{m_e c^2} + \frac{kT_p}{m_p c^2} \right)^{3/2} \quad (25)$$

where T_e and T_p are the electron and proton temperatures, and $\ln \Lambda \sim 20$ is the Coulomb logarithm. Coulomb collisions between proton and electrons allow electrons to be heated for a time t_{ep} . The additional energy gained by the electrons is radiated on a cooling timescale. This corresponds to an additional luminosity

$$L'_{x,p} \simeq \frac{\epsilon' \epsilon_p}{t'_{\text{ep}}} \quad (26)$$

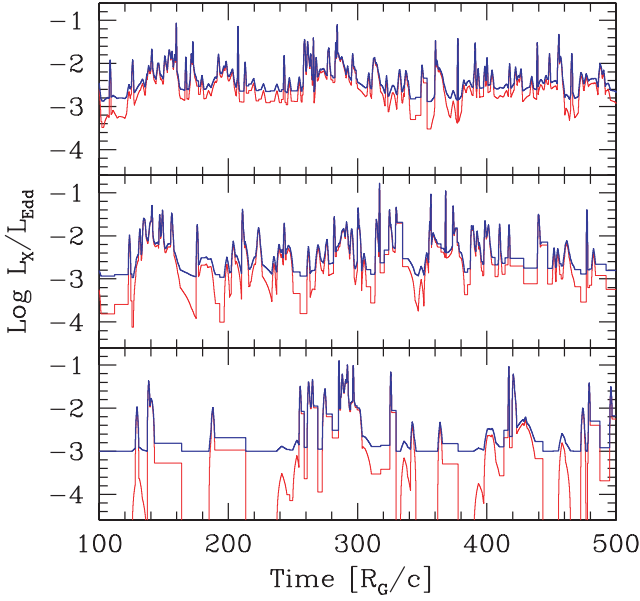


Fig. 4. Light curves of the integrated X-ray luminosity (in units of the Eddington one) corresponding to numerical simulations, as discussed in the text. Thin lines corresponds to the power emitted by shell-shell collisions. To this, we have added a constant luminosity (0.1% Eddington) and the sum is shown by the thick solid lines. Note that these light curves take into account the total number of shells which an observer sees “on” at a given time. The three cases differ only for the average time interval between the blobs, which is 4, 8 and 16 R_G/c from top to bottom. Note that these results are scale-invariant: the light curve does not change changing the black hole mass.

where ϵ_p is the fraction of dissipated energy heating the protons. We then transform $L'_{x,p}$ as before, taking into account beaming and gravitational redshift. In our cases t'_{cross} is almost always shorter than t'_{ep} , and consequently $L'_{x,p}$ is almost always smaller than L'_x , but it lasts longer, somewhat smoothing the lightcurve.

For the simulations shown in Fig. 4 and in Fig. 5 we have assumed:

- $\langle\beta_0\rangle = 0.5$; $\sigma_{\beta_0} = 0.2$; Gaussian distribution;
- $\langle\Delta t\rangle = 4, 8, 16 R_G/c$; Poisson distribution;
- launching site $R_0 = 5R_g$ equal for all blobs;
- blob size $r_j = 4R_g$ equal for all blobs;
- blob width $\Delta r_j = r_j$ equal for all blobs;
- the blobs do not expand nor contract;
- the jet initial kinetic luminosity L_j equal to the radiative accretion disk luminosity, both being equal to $0.1 L_{\text{Edd}}$;
- maximally spinning black hole;
- $\epsilon_e = 1/3$; $\epsilon_p = 1/3$ for all blobs;
- $\cos\theta = 0.5$.

Clearly, some of these assumptions are not fully justified physically, but have been done just for ease of computation. In particular, one expects that the blob size and width change during the blob trajectory; one furthermore expects that the launching size is not the same for all blobs.

Figure 4 shows the light curves of the bolometric luminosity for three cases, corresponding to $\langle\Delta t\rangle = 4, 8, 16 R_G/c$ (from

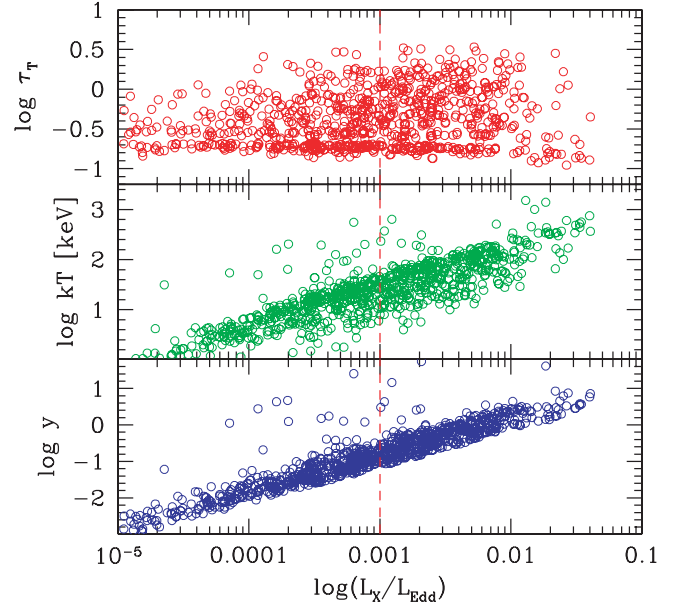


Fig. 5. Thomson scattering optical depth, plasma temperature (in keV) and Comptonization y parameter as a function of integrated X-ray luminosity produced in single collisions for the case corresponding to the top panel of Fig. 4. The dashed vertical line corresponds to 0.1% of the Eddington luminosity which we have assumed to be constant.

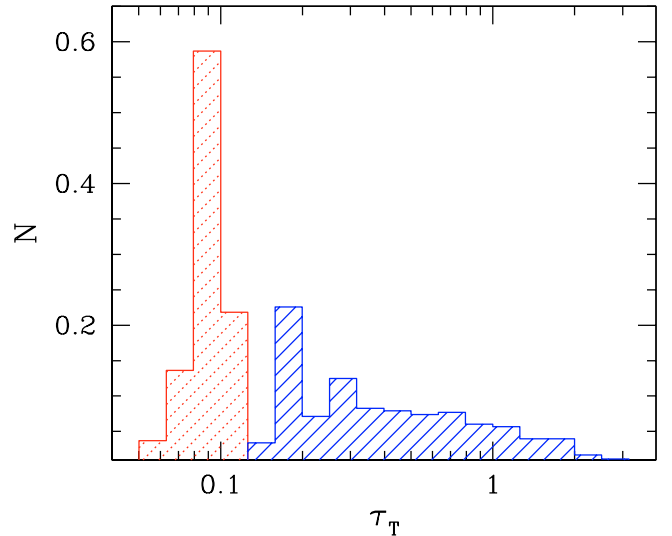


Fig. 6. When a blob is launched, it has an optical depth belonging to the distribution shown by the dotted histogram. The other histogram shows the distribution of τ_T soon after each collision.

top to bottom). Being an intrinsically intermittent process, the resulting light curves (thin lines) show a very large range of variability (the luminosity can virtually vanish for some time interval). This corresponds to the case of a completely “on and off” mechanism, i.e. there is a vanishing particle density between the launched blobs. We consider this unphysical, even if useful for estimating the radiated power in the way we have discussed above. A more sophisticated treatment should take into account a “smoother” behavior of the central engine, with density and velocity profiles described by smooth functions. While this is referred to future work, the general effect on the

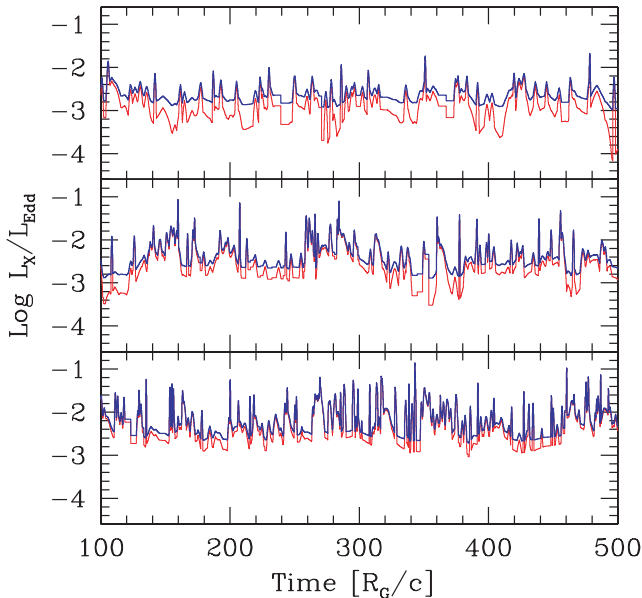


Fig. 7. Light curves of the integrated X-ray luminosity (in units of the Eddington one) corresponding to numerical simulations. The three cases differ for the average initial average velocity, which is 0.3, 0.5 and 0.7 c , from top to bottom. The average time interval between consecutive shell ejection is $\langle \Delta t \rangle = 4R_g$. All other parameters are the same as in Fig. 4.

light curve will be to allow some of the energy carried by the blobs (that in a more physical scenario can be thought as overdense regions) to be dissipated all along the jet, and not only during collisions with other overdense region. This emission may correspond to a minor fraction of the luminosity produced during each collision, but it should be much more continuous.

To partly account for that we have added, in Fig. 4 and in Fig. 7, a constant luminosity equal to 0.1 per cent of the Eddington value. The thick solid lines are the sum of this contribution and the contribution produced by the shell-shell collisions.

The three different curves in Fig. 4 show the effect to change the time interval between the launching of blobs. For increasing time intervals, less spikes per unit time are produced and the overall process becomes less efficient, since there are less collisions.

Note that, in agreement with our simple estimates, the average emitted luminosity (at least for short Δt) is around a few per cent of the jet initial kinetic power.

Figure 5 shows the optical depth τ_T , the electron temperature kT and the Comptonization y parameter as a function of the luminosity produced in each collision (i.e. this is not the sum over the “on” shells used in Fig. 4). For reference, we have drawn a vertical line corresponding to 0.1 per cent of the Eddington luminosity and corresponding to the stationary component assumed above. For this case we have assumed $\Delta t = 4R_g/c$ as in the top panel of Fig. 4. As can be seen, when the luminosity is relevant (i.e. $L_x^{\text{obs}} \sim 10^{-1}L_j = 10^{-2}L_{\text{Edd}}$), we have optical depths between 0.5 and 2, temperatures around 100 keV and $y \sim 1$. For this case we obtain values of the optical

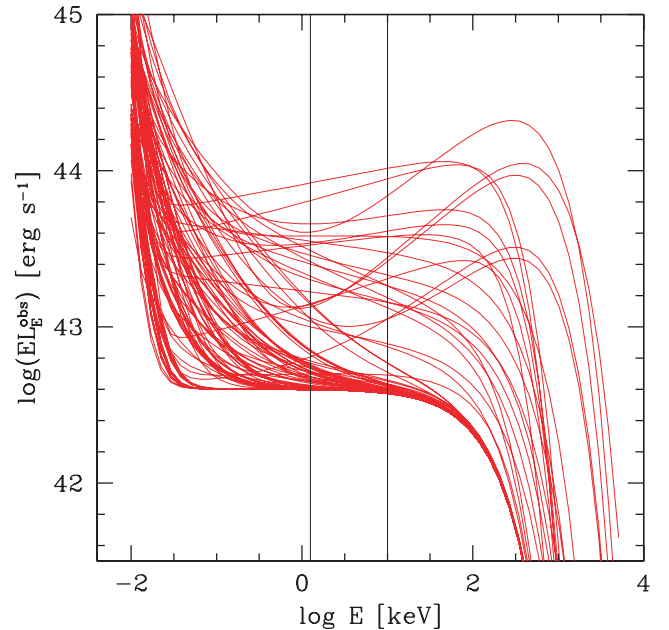


Fig. 8. Example of time dependent spectra for the case illustrated in the top panel of Fig. 4, assuming a black hole of 10^8 solar masses. Spectra are calculated every $2.7 \times 10^{-2}R_g/c$, but for clarity the figure shows spectra every $0.53R_g/c$ (i.e. every 800 s for a black hole of 10^8 solar masses), from $t/(R_g/c) = 240$ and 300. Vertical lines mark the 1–10 keV band.

depth which are a few times larger than the initial ones, due to the previous collisions done by the shells, as shown in Fig. 6.

5.1. Observed spectra

Since we can calculate the optical depth and temperature for each shell-shell collision, we can calculate the emitted spectrum assuming thermal Comptonization as the radiative process. To this end we use the analytical formulae of Titarchuk & Mastichiadis (1994), and assume that the soft radiation field is a blackbody peaking at some energy ϵ_0 . For all cases discussed in the following, we have assumed $\epsilon_0 = 5$ eV. For each observing time, we sum up the spectra of the “on” shells, including the contribution of the steady component, whose bolometric luminosity amounts to the 0.1 per cent of the Eddington luminosity. We have assumed that the spectral shape of this steady component is $F(\nu) \propto \nu^{-1}e^{-\nu/\nu_c}$, with $h\nu_c = 150$ keV.

This specific chosen spectral index may account for the contribution of the hot corona, above the accretion disk, while it is not clear if it can be directly associated to the jet generation process (e.g., to a particle injection in the jet smoother than the assumed on-off mechanism). In this latter case the usual feedback process operating in the hot corona model, fixing the spectral index close to unity, does not work. In fact, when the power of the steady component is much smaller than the luminosity of the disk, there is no feedback, and the Comptonization spectrum should be much steeper than unity.

Figure 8 shows some example of spectra born out from our simulations. They correspond to the case shown in the top panel of Fig. 4, assuming a black hole of 10^8 solar masses. Spectra

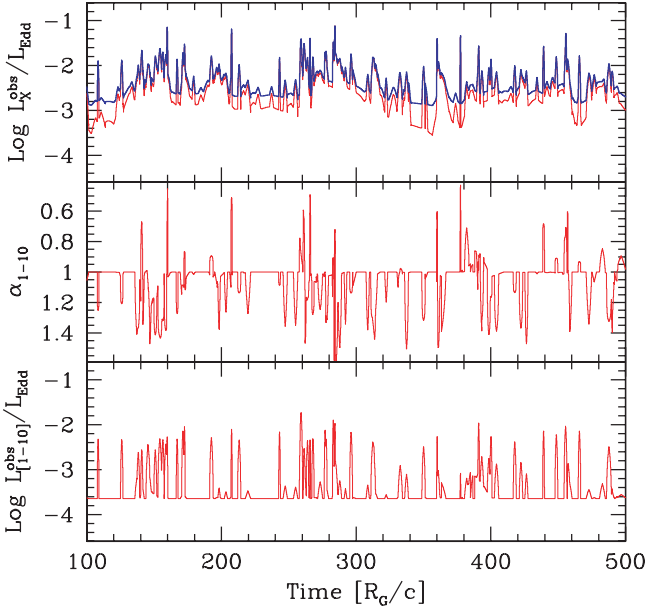


Fig. 9. Light curves of the integrated X-ray luminosity (in units of the Eddington one) corresponding the top panel of Fig. 4, the light curve of the spectral index and flux between 1 and 10 keV. We have assumed that the spectral shape of the steady component is $F(\nu) \propto \nu^{-1} e^{-\nu/\nu_c}$.

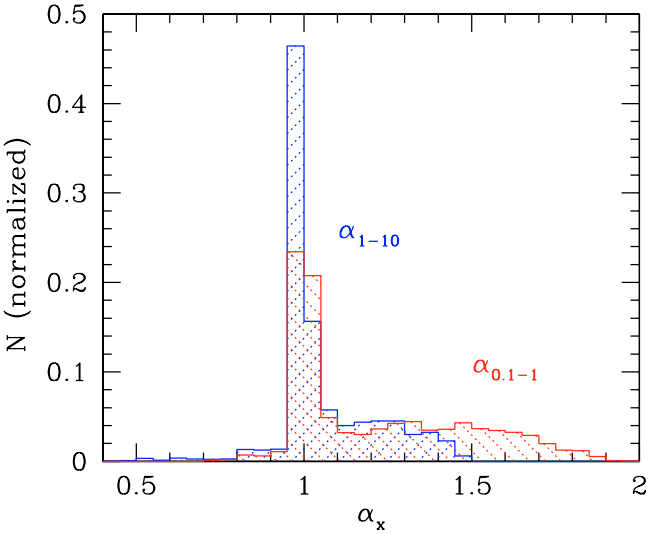


Fig. 10. Histograms of the soft (0.1–1 keV) and hard (1–10 keV) X-ray spectral indices for the case shown in Fig. 9.

are calculated every 40 s, but are shown every 800 seconds (corresponding to $0.53R_g/c$), for clarity, from $t/(R_g/c) = 240$ to $t/(R_g/c) = 300$. Figure 9 shows again the light curve corresponding to the top panel of Fig. 4, together with the associated 1–10 keV spectral index, $\alpha_{[1-10]}$ and the light curve of the 1–10 keV flux. Figure 10 shows the histograms of $\alpha_{[1-10]}$ and the softer spectral index $\alpha_{[0.1-1]}$ (between 0.1 and 1 keV).

By construction, a spectral index different from unity corresponds to the jet emission dominating over the steady component. Most of the time, the observed slopes corresponding to the jet emission are steeper than unity (as shown in Fig. 10), and even more so at lower frequencies.

5.2. Trends

In this section we summarize the results of the survey of the parameter space aimed to test the sensitivity of our results to our assumptions. We indicate the values of the parameters we have changed, all other parameters have values equal to the case shown in the top panel of Fig. 4.

- **Initial velocity** – Figure 7 shows the effect of changing the average initial velocity of the ejected shell ($\langle\beta_0\rangle = 0.3, 0.5$ and 0.7 from top to bottom). It can be seen that an increase of the average initial velocity has the effect to increase the density of spikes and their average luminosity. Increasing the average velocity, in fact, increases the average number of collisions per unit time and the average efficiency of each collision. The overall process becomes more efficient.
- **Launching site** – Increasing the launching site from the black hole (we tried $R_0 = 3, 5$ and $7 R_g$) the bolometric and the 1–10 keV light curves becomes more spiky, with the jet dominant (in the 1–10 keV band) an increasing number of times over the steady component. The net effect is, basically, the same as increasing the initial velocity.
- **Shell size** – Increasing Δr_j (we tried $\Delta r_j = 1, 2$ and $4 R_g$, always with $r_j = 4R_g$), the light curve becomes slightly less spiky, as the duration of the collisions is proportional to Δr_j .
- **Spin of the black hole** – We have found negligible differences between a maximally rotating Kerr and a Schwarzschild black hole for the launching site $R_0 = 5R_g$. There is still a negligible difference for the case $R_0 = 3R_g$ and $\beta_0 = 0.7$.
- **Ratio of jet to disk power** – We consider this as the most important parameter. As the jet power increases, the jet emission becomes (obviously) more and more dominant over the steady emission, and the average spectral index flattens, to become flatter than unity for $L_j \sim 20L_d$. For larger values of the jet power, the radiation produced by the jet is larger than the luminosity radiated by the disk. The radiation coming from the jet and reprocessed by the disk can no longer be neglected, and our treatment becomes invalid. However, in this case, the power in the optical–UV and in the X-ray bands are comparable, in contrast with the majority (albeit not all) of Seyfert galaxies.

6. Summary and discussion

We have explored the possibility that all Active Galactic Nuclei form jets or outflows, with a range of velocities, but with a power which is comparable to the power extracted by the accretion process. We have then assumed that in most cases (corresponding to radio-quiet sources) the jets are launched with velocities smaller than the escape velocity. Mainly for simplicity, but also in analogy with the “internal shock” scenario proposed to work in radio-loud sources and in gamma-ray bursts, we have further assumed that the central engine works intermittently, producing shells or blobs. A shell with $\beta < \beta_{\text{esc}}$ will reach a maximum distance from the hole, then stop and invert its motion, and may eventually collide with the successive shell. In this case the bulk kinetic energy of the two shells is dissipated, and the fraction of it which is given to electrons

can be transformed into radiation. The accelerated electrons are embedded in the dense radiation field produced by the accretion disk: they cool rapidly by the inverse Compton process, producing the X-ray continuum. Simple energy balance is sufficient to estimate the Comptonization parameter as a function of the power dissipated by the colliding blobs and the disk luminosity. By construction, the shells are moving with velocities smaller than the escape speed, yet they carry a power which is comparable to that extracted by accretion. This implies that the shells are “heavy”. They cannot be formed by electron-positron pairs only, because in this case the corresponding optical depth is so large that most of them annihilate in less than a dynamical time. The required density in protons and the accompanying electrons is large enough to limit the importance of pairs not only as energy carriers, but also as scatterers.

The main aim of this paper is to investigate the general properties of the proposed idea, to check if it can work at least at the first order of approximation.

Our “aborted jet” scenario is not necessarily alternative to the popular “disk-corona” model. Both processes could be active and contribute to the formation of the high energy continuum in the same source. On the other hand we would like to stress that in our proposed scenario the source of energy could be the spin of the hole, besides accretion. Pushing this possibility to the limit (i.e. all the high energy emission produced by AGNs comes from the rotational energy of their black hole), would result in the remarkable fact that it is the black hole spin, rather than accretion, which produces the bulk of the X-ray background. It is then instructive to isolate the “aborted jet” process in order to find ways to confirm or falsify this scenario.

One of the clearest difference with the disk-corona model is that the dissipation of energy should occur along the axis of rotation of the black hole. This implies that the X-ray flux coming from the colliding shells will illuminate preferentially the inner part of the disk, especially when they collide close to the hole. This may solve the problem of the formation of the strong red wings of the relativistic iron line observed in MCG-6-30-15 (Wilms et al. 2001), which requires an “illuminator” emissivity strongly increasing towards the black hole. It should be noted that we have neglected, for simplicity, the light bending due to the strong gravity (see e.g. Martocchia et al. 2002), which results in an enhanced illumination of the innermost disk regions. The illumination could be further enhanced by anisotropic Compton scattering (since the seed photons are coming from the disk, more inverse Compton radiation is channeled back towards the disk than along the viewing angle, see e.g. Ghisellini et al. 1991; Malzac et al. 1998). Another cause of anisotropy is beaming of the X-ray radiation, which is preferentially emitted towards the accretion disk in efficient shell-shell collisions. According to our simulations, in fact, the most efficient collisions are between massive blobs coming back to the disk and having already experienced some collisions, and newly generated blobs moving in the opposite direction. While this may help explaining the large equivalent widths of Fe lines observed in a few cases (notably MCG-6-30-15), it is apparently at odds with the relative paucity of relativistic iron lines observed by XMM-Newton (e.g. Reeves et al. 2003). However, it should be noted that the increase of illuminating X-ray

photons may result in a significant ionization of the innermost regions of the accretion disc, making predictions on the iron line intensity less straightforward (e.g. Nayakshin & Kazanas 2002, and references therein). Detailed calculations of the iron line properties are beyond the scope of this paper, and are deferred to a future work.

We note that an important piece of information may come from the observations of the Compton reflection continuum and iron line in radio-loud sources. If the jet in these sources is successful, in fact, it should not illuminate much of the accretion disk, and therefore these objects should have weaker reflection features produced by the corona only. This seems indeed to be the case (e.g. Grandi et al. 2002, and references therein). Then the equivalent width of the fluorescent iron lines in radio-galaxies may measure the importance of the corona with respect to the jet in producing the thermal X-ray continuum, once the data are purified from all other additional contributions (e.g. the non thermal radiation from the jet).

The spectral index of the jet emission, calculated in our simulations, is generally steeper than the average spectral index observed in Seyfert galaxies (i.e. $\alpha_x \sim 1$). As it is, our model requires therefore the presence of a steadier component, with the “right” spectral index, contributing to the X-ray band. This steady component should have a bolometric luminosity which is, on average, smaller than the average power of the jet, even if its relative contribution in the 1–10 keV band is more important. The steep jet emission, when contributing notably to the 1–10 keV band, would steepen the overall spectral index and increase the flux. It would then produce a “steeper when brighter” behavior as observed in Seyfert galaxies (e.g. Zdziarski et al. 2003). Occasionally, instead, the jet emission is both dominant and characterized by a flat spectrum, and we have then the opposite behavior, i.e. “harder when brighter”, but this occurs more rarely.

As it is, our model explains the X-ray properties of Narrow Line Seyfert 1 galaxies (Boller et al. 1996; Brandt et al. 1997; Cancelliere & Comastri 2002). These sources are in fact characterized, on one hand, by a 2–10 keV spectral index between 1 and 1.5 (and an even steeper spectrum in the softer band), and, on the other hand, by a short term, large amplitude variability. It is then possible that the main difference between Narrow Line Sey1 (including in this class also sources like MCG-6-30-15 which have broad lines but in X-rays behaves like NLSy1s) and classical Seyferts is the ratio between jet and disc/corona emission. It is worth noting that NLSy1 are widely believed to have a larger L/L_{Edd} ratio than classical Seyferts, which again can be explained by an enhanced jet emission. If this is true, one could speculate that the physical parameter behind the NLSy1 X-ray behaviour is not (or at least not only) the accretion rate, as usually supposed, but the presence of a more powerful aborted jet.

Regarding broad line, classical Seyfert 1 galaxies, we should however consider that our model neglects, for simplicity and ease of calculation, a few important physical effects. One of these concerns light bending, important when the emitting spot is very close to the black hole. This effect is expected to change the observed X-ray luminosities only by a factor of a few (Martocchia et al. 2002), but that can nevertheless be very important for a detailed study of spectral evolution.

Indeed, a different degree of light bending and gravitational redshift corresponding to different heights of the illuminator above the black hole can explain the puzzling temporal behavior of MCG–6–30–15, where the continuum and iron line variabilities are decoupled (Miniutti et al. 2003).

Another important effect, neglected here, is the feedback between the luminosity produced by the jet and the disk emission, important for large ratios between the jet and the disk powers. In these cases the radiation reprocessed by the disk can become important and introduce the same kind of feedback which makes the hot corona model to work, producing spectral indices close to unity in the X–ray band.

Finally, we would like to comment about the difference between radio–loud and radio–quiet sources. In our scenario, this is mainly a difference in mass loading, coupled with a possible difference in jet power. The central engine in radio–loud sources succeeds in accelerating jets at speeds larger than the escape velocity: in these sources the jet power can dominate the total energetics (as in BL Lac objects), and the outflow mass rate is of the order of a per cent of the accretion rate. The “jet” of radio–quiet sources may not be much less powerful than in radio–loud objects, if it contributes significantly to the formation of the X–ray flux. What should be different is the outflowing mass rate, which must be greater in radio–quiet objects, making their “jets” move slower. If all jets are powered by the extraction of rotational energy from a spinning black hole, it is then possible that it is this mechanism, and not accretion, to be responsible for all the high energy radiation produced by AGNs (i.e. all the X–ray and the γ –ray flux).

It is also possible that a specific source, usually radio–quiet, occasionally may launch “successful” shells, with relativistic speeds. However, these “successful jet episodes” must be rare in AGN, since we rarely see “fossil” long lived weak radio lobes in not jetted sources. This may occur more often in galactic micro–quasars, and be associated with the major radio–flares. The bulk Lorentz factor associated with major radio events in GRS 1915+105 is relatively small, perhaps suggesting that, when radio–weak, the jet is not successfully launched because it does not attain bulk speeds larger than the escape velocity. These sources may therefore be the “missing link” between radio–loud and radio–weak sources, changing from time to time from one class to the other.

Acknowledgements. We thank M. Abramowicz, V. Karas and D. Malesani for useful discussions and the anonymous referee for having been at the same time severe and encouraging. We thank MIUR and ASI for funding.

References

- Blandford, R. D. 1990, in *Active Galactic Nuclei. Saas–Fee Advanced Course 20* (Springer–Verlag)
- Boller, T., Brandt, W. N., & Fink, H. 1996, *A&A*, 305, 53
- Brandt, W. N., Mathur, S., & Elvis, M. 1997, *MNRAS*, 285, L25
- Cancelliere, F., & Comastri, A. 2002, *Proc. of the 5th Italian AGN Meeting, Inflows, Outflows and Reprocessing around black holes* [astro-ph/0301163]
- Elvis, M., Risaliti, G., & Zamorani, G. 2002, *ApJ*, 565, L75
- Fabian, A. C., Vaughan, S., Nandra, K., et al. 2002, 335, L1
- Falcke, H., & Biermann, P. L. 1995, *A&A*, 293, 665
- Frank, J., King, A., & Raine, D. 1985, *Accretion power in Astrophysics* (Cambridge, UK: Cambridge University Press)
- Ghisellini, G., George, I. M., Fabian, A. C., & Done, C. 1991, *MNRAS*, 248, 14
- Ghisellini, G., Haardt, F., & Fabian, A. C. 1993, *MNRAS*, 263, L9.
- Ghisellini, G., Haardt, F. & Svensson, R. 1998, *MNRAS*, 297, 348
- Ghisellini, G. 1999, *Astronomische Nachrichten*, 320, 232
- Grandi, P., Urry, C. M., & Maraschi, L. 2002, *New Ast. R.*, 46, 221
- Guainazzi, M., Matt, G., Molendi, S., et al. 1999, *A&A*, 341, L27
- Haardt, F., & Maraschi, L. 1991, *ApJ*, 380, L5
- Haardt, F., & Maraschi, L. 1993, *ApJ*, 413, 507
- Haardt, F., Maraschi, L., & Ghisellini, G. 1994, *ApJ*, 432, L95
- Haardt, F. 1994, Ph.D. Thesis, SISSA, Trieste
- Henri, G., & Petrucci, P. O. 1997, *A&A*, 326, 87
- Ivezic, Z., Menou, K., Knapp, G. R., et al. 2002, *AJ*, 124, 2364
- Iwasawa, K., Fabian, A. C., Reynolds, C. S., et al. 1996, *MNRAS*, 282, 1038
- Lynden Bell, D. 2001, in *The Central Kpc of Starbursts and AGNs: The La Palma Connection*, ed. J. H. Knapen, J. E. Beckman, I. Shlosman & T. J. Mahoney, *ASP Conf. Ser.*, 249, 212 [astro-ph/0203480]
- Malzac, J., Jourdain, E., Petrucci, P. O., & Henri, G. 1998, *A&A*, 336, 807
- Martocchia, A., Matt, G., & Karas, V. 2002, *A&A*, 383, L23
- Merloni, A., & Fabian, A. C. 2001, *MNRAS*, 321, 549
- Miller, J. M., Fabian, A. C., Wijnands, R., et al. 2002a, *ApJ*, 570, L69
- Miller, J. M., Ballantyne, D. R., Fabian, A. C., & Lewin, H. G. 2002b, *MNRAS*, 335, 865
- Miniutti, G., Fabian, A. C., Goyder, R., & Lasenby, A. N. 2003, *MNRAS*, submitted [astro-ph/0307163]
- Moderski, R., Sikora, M., & Lasota, J–P. 1998, *MNRAS*, 301, 142
- Nayakshin, S., & Kazanas, D. 2002, *ApJ*, 567, 85
- Perola, G. C., Matt, G., Cappi, M., et al. 2002, *A&A*, 389, 802
- Petrucci, P. O., Haardt, F., Maraschi, L., et al. 2001, *ApJ*, 556, 716
- Pozdnyakov, L. A., Sobol, I. M., & Sunyaev, R. A. 1983, *Sov. Sci. Rev., Sect. E: Astrop. and Space Physics Rev.*, 2, 189
- Rees, M. J. 1978, *MNRAS*, 184, P61
- Rees, M. J., & Mészáros, P. 1992, *MNRAS*, 258, P41
- Rees, M. J., & Mészáros, P. 1994, 1994, *ApJ*, 430, L93
- Reeves, J. 2003, in *Active Galactic Nuclei: from Central Engine to Host Galaxy*, ed. S. Collin, F., Combes, & I. Shlosman, *ASP Conf. Ser.*, in press [astro-ph/0211381]
- Sari, R., & Piran, T. 1997, *MNRAS*, 287, 110
- Spada, M., Ghisellini, G., Lazzati, D., & Celotti, A. 2001, *MNRAS*, 325, 1559
- Stepney, S. 1983, *MNRAS*, 202, 467
- Svensson, R. 1984, *MNRAS*, 209, 175
- Tanaka, Y., Nandra, K., & Fabian, A. C. 1995, *Nature*, 375, 659
- Titarchuk, L., & Mastichiadis, A. 1994, *ApJ*, 433, L33
- Ulvestad, J. S. 2003, in *Radio Astronomy at the Fringe*, *ASP Conf. Ser.*, Vol. XXV, ed. J. A., Zensus, M. H., Cohen, & E., Ros, in press [astro-ph/0301057]
- Vokrouhlický, D., & Karas, V. 1991, *A&A*, 252, 835
- Walter, R., & Fink, H. H. 1993, *A&A*, 274, 105
- White, R. L., Becker, R. H., Gregg, M. D., et al. 2000, *ApJS*, 126, 133
- Wilms, J., Reynolds, C. S., Begelman, M. C., et al. 2001, *MNRAS*, 328, L27
- Zdziarski, A. A., Gilfanov, M., Lubinski, P., & Revnivtsev, M. 2003, *MNRAS*, 342, 355